Pt atoms adsorbed on TiO_2(110)-(1 × 1) studied with noncontact atomic force microscopy and first-principles simulations

Delia Fernández-Torre,[1,2] Ayhan Yurtsever,[3,4,*] Jo Onoda,[3] Masayuki Abe,[5] Seizo Morita,[3,4] Yoshiaki Sugimoto,[3] and Rubén Pérez[1,6,†]

[1]*Departamento de Física Teórica de la Materia Condensada, Universidad Autónoma de Madrid, E-28049 Madrid, Spain*

[2]*Instituto de Estructura de la Materia, CSIC, Serrano 121, 28006 Madrid, Spain*

[3]*Graduate School of Engineering, Osaka University, 2-1 Yamada Oka, Suita, Osaka 565-0871, Japan*

[4]*The Institute of Scientific and Industrial Research, Osaka University, 8-1 Mihogaoka, Ibaraki, Osaka 567-0047, Japan*

[5]*Graduate School of Engineering Science, Osaka University, 1-3 Machikaneyama, Toyonaka, Osaka 560-8531, Japan*

[6]*Condensed Matter Physics Center (IFIMAC), Universidad Autónoma de Madrid, E-28049 Madrid, Spain*

(Received 17 November 2014; revised manuscript received 15 January 2015; published 2 February 2015)

We have studied the local properties of single Pt atoms adsorbed on hydroxylated TiO_2(110)-(1 × 1) by combining noncontact atomic force microscopy (nc-AFM) and first-principles calculations. Room-temperature high-resolution nc-AFM images for the most frequently observed contrast modes reveal bright and elongated protrusions that can be traced back to the Pt atoms, and that are centered on the fivefold coordinated titanium rows, confined between two bridging oxygen rows. These observations are in line with the theoretical results, as the lowest energy sites for the Pt atom on the TiO_2(110) surface are in the neighborhood of the titanium rows, and high energy barriers have to be overcome to displace the Pt atom over the bridging oxygen rows. Single Pt atoms can be distinguished from H adsorbates (OH defects) due to their characteristic shape and binding site and, because they appear as the brightest surface features in all of the contrast modes. Force spectroscopy data over the protrusion and hole imaging modes and the corresponding tip-sample forces, simulated with O and OH terminated TiO_2 nanoclusters, provide an explanation for this puzzling result in terms of the intrinsic strength of the interaction with the Pt adatom and the adatom and tip apex relaxations induced by the tip-sample interaction. These imaging mechanisms can be extended to other electropositive metal dopants and support the use of nc-AFM not only to characterize their adsorption structure but also to directly probe their chemical reactivity.

DOI: 10.1103/PhysRevB.91.075401 PACS number(s): 68.47.Gh, 68.37.Ps, 07.05.Tp

I. INTRODUCTION

Pt/TiO_2 materials are among the most important industrial heterogeneous catalysts, with applications including the photochemical splitting of water [1] and the photocatalytic conversion of CO_2 and water to hydrocarbon fuels [2]. In all of these systems, Pt nanostructures play a key role as a cocatalyst. Many studies have concentrated on the development of growth methods to achieve highly active Pt catalysts within a size range of a few nanometers [3,4]. The driving force for this research effort has been the fact that the catalytic activity of these nanostructures for different chemical processes, including the ones mentioned above and others like CO oxidation reactions, dramatically increases with a reduction of the size of the supported metal nanoparticles. Recent experiments [5] have confirmed that this trend extends into the subnanometer scale.

The reactivity of these small Pt structures is controlled by quantum size effects caused by the small number of atoms composing the metal particles. Understanding the basic catalytic mechanisms and improving their performance has driven an important research effort into model systems, like Pt individual atoms and nanoparticles on the rutile TiO_2(110)-(1 × 1) surface, that can be studied with powerful surface science techniques and characterized at the atomic scale. Scanning tunneling microscopy (STM) has been the tool of choice to gather information on the structure, adsorption configuration, and electronic properties of individual Pt atoms and small metal clusters deposited on TiO_2(110) [6,7]. Recently, direct atomic-resolution images of individual Pt atoms adsorbed on TiO_2 (110) surfaces using aberration-corrected scanning transmission electron microscopy have been reported [8]. The subangstrom spatial resolution achieved in this work, together with density functional theory (DFT) calculations, has revealed the interaction of Pt atoms with a class of surface defects, vacancies of basal threefold coordinated oxygen atoms that are located in the same plane as the Ti atoms, that have not been identified in previous STM studies [9]. This study concludes that the most favorable Pt adsorption site is not on the oxygen vacancy on the top bridging oxygen rows predicted by previous DFT studies [10–12], but on these new vacancy sites.

Recent progress in frequency modulation atomic force microscopy (FM-AFM) [13], commonly known as noncontact AFM (nc-AFM), has shaped it into a powerful alternative tool to image and characterize the Pt/TiO_2(110) system. nc-AFM has contributed significantly to the atomic-scale understanding of metal oxide surfaces including their defects and adsorbates [14–17]. At variance with other oxides, TiO_2 displays qualitatively different nc-AFM contrasts depending on the chemical composition and structure of the tip apex used to imagine it [18–23]. These different imaging modes can be identified by the location of the most common surface defects, oxygen vacancies, and hydroxyl (OH) groups and their associated contrast. Two types of contrasts, the protrusion and the hole imaging modes, are the most frequent. The

*ayhan@afm.eei.eng.osaka-u.ac.jp
†ruben.perez@uam.es

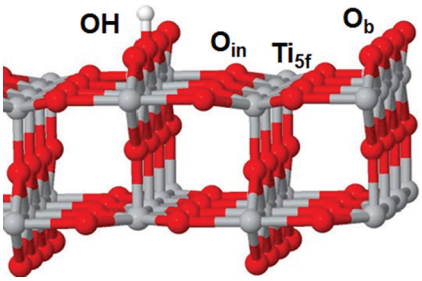

FIG. 1. (Color online) Ball-and-stick structure of the hydroxylated TiO_2(110) surface, highlighting the important O_b, Ti_{5f}, and O_{in} sites and the common hydroxyl (OH) defects. O (Ti) atoms are displayed as red (gray) balls; H atoms as white.

protrusion mode is characterized by alternating rows of bright fivefold coordinated titanium (Ti_{5f}) atoms and dark twofold coordinated bridging oxygen (O_b) atoms imaged as bright and dark, respectively. OH defects, sitting on the O_b rows, show up as small bright protrusions [see Fig. 2(a)]. A ball-and-stick representation of the surface structure with indication of the different atomic sites (O_b, Ti_{5f}) and OH defects is depicted in Fig. 1. The contrast in the hole imaging mode is the reversal of the previous one: O_b rows look bright; Ti_{5f} rows and OH surface defects look dark. Apart from the frequent protrusion and hole modes, a third kind of contrast, the neutral mode, has also been reported [18]. A neutral mode image differs from a hole mode one on the contrast of the OH defects that are imaged as brighter protrusions on the bright O_b rows, so the nc-AFM topography is close to the real topography of the surface. These different contrasts have been explained by assuming that the tip-sample interactions are mainly electrostatic and controlled by the charge distribution at the tip apex: a negatively charged tip for the protrusion mode and a positively terminated tip for the hole contrast. The fact that electropositive ions like the Ti_{5f} and the OH defects are imaged bright in the protrusion mode may suggest that electropositive adsorbates as Pt would be difficult to distinguish from these chemical species on the surface.

In this work, we have combined nc-AFM imaging and force spectroscopy at room temperature (RT) with *ab initio* DFT simulations to study individual Pt atoms adsorbed on the hydroxylated rutile TiO_2 (110) surface [h-TiO_2(110)]. Pt atoms can be identified as the brightest protrusions in all the different contrast modes. Their elongated shape is consistent with the calculated potential energy surface that shows that Pt atoms are confined by the bridging oxygen rows but are quite mobile parallel to them. Force spectroscopy results for the protrusion and hole imaging mode can be explained in terms of the same O- and OH-terminated tips proposed in our recent study of the bare TiO_2(110) surface [23]. The calculations help us to identify the contrast mechanisms for the different imaging modes, discuss the crucial role of the adatom and tip apex relaxations, and explain why we can differentiate electropositive species as Pt adatoms from the OH groups.

The rest of the paper is organized as follows. In Sec. II A we briefly discuss the experimental setup and conditions, while in Sec. II B we specify the computational details. We will present our main results and discuss them in Sec. III, treating separately the nc-AFM images (Sec. III A) and the tip-sample force curves (Sec. III B). Finally, we will end by highlighting the main conclusions in Sec. IV.

II. METHODS

A. Experiment

Experiments were carried out using a homebuilt ultrahigh vacuum (UHV) nc-AFM operated at RT with a base pressure of at least 5×10^{-11} Torr. The microscope was operated using the frequency modulation detection mode, keeping the cantilever oscillation amplitude constant [24]. Conductive Si cantilevers were cleaned via Ar^+ ion sputtering to remove the native oxide layer and other contaminants prior to imaging and characterizations. A rutile TiO_2(110) substrate (Shinkosha) was prepared by repeated cycles of Ar^+ ion sputtering (2 keV, 3×10^{-6} Torr) for about 6 min at RT followed by annealing at approximately 1000 K for about 10 min. When the substrate was cooled down to RT after the final annealing process, Pt atoms were evaporated by resistively heating a Ta wire coiled up with high purity Pt (99.995%). Prior to deposition, the source was outgassed in UHV at high temperatures, and the typical Pt adsorption condition was adjusted to a heating current of $\sim$7.6 A and adsorption time of at least $\sim$2 min. The sample was then transferred into an observation chamber and scanned with a freshly prepared conductive Si cantilever. The OH defects on TiO_2(110) surface were spontaneously created from the dissociation of water molecules (from residual background water in UHV chamber) over the oxygen vacancy sites by transferring H atom to a neighboring O_b site. It is well known that the transformation from a freshly prepared surface (reduced TiO_2) to a fully hydroxylated one occurs within 2–3 h. By keeping the freshly prepared surface in UHV for several hours, all of the oxygen vacancies are occupied by OHs. It has been known that the morphology of Pt atoms is very sensitive to the hydroxylation state of an oxide surface [25]. Therefore, the oxidation state of the bare TiO_2(110) surface was carefully investigated before exposing to a Pt atom evaporation source. Force spectroscopy measurements were carried out by recording the frequency shift (Δf) with respect to the resonant frequency (f_0) as a function of the tip-sample distance (z). These $\Delta f(z)$ curves were then converted to force-distance curves using the method described in Ref. [26]. Then, the short-range interaction forces were obtained by subtracting the long-range forces from the total forces. Detailed information related to force spectroscopy measurement and the method for the extraction of the long-range forces from total forces can be found in Ref. [23]. The bias voltage (Vs) applied to the sample surface, with the tip held at ground potential, was adjusted to minimize the long-range electrostatic forces. A sample bias in the range of 0.4–2 V was applied in the course of our experiments.

B. Computational details

All calculations have been performed at the DFT level using the Perdew-Burke-Ernzernhof (PBE) [27] exchange-correlation functional as implemented in VASP 5.2.12 [28], combined with the projector-augmented-wave method and a plane-wave cutoff of 400 eV. Previous theoretical works found that spin polarization is negligible in the Pt/TiO_2(110) system

[10,11], and we have confirmed it in our preliminary tests. To study the adsorption of single Pt atoms on TiO_2(110)-(1 × 1), we started by building a 2 × 1 (5.9 Å × 6.6 Å) supercell and sampling the Brillouin zone with a 2 × 2 Monkhorst-Pack k-point mesh. For this system, we tested the convergence of the relative energies between different Pt adsorption sites as a function of slab thickness, finding that an asymmetric slab of four trilayers, with the two lowermost trilayers fixed to their bulk positions, was well converged compared to thicknesses of up to seven trilayers. To simulate the conditions of the nc-AFM experiments, we have considered a significantly larger 4 × 2 supercell (11.9 Å × 13.2 Å) in order to minimize the lateral interactions between the periodic images of our model tips. In these calculations we have reduced the Brillouin zone sampling to only the Γ point. The lattice parameter perpendicular to the surface was chosen so that a vacuum of at least 7 Å is left between the upper part of the model tip and the lower part of the slab for the largest tip-sample distance considered. To calculate the tip-sample forces we approach our tip models to the surface in a quasistatic way, in small steps of 0.25 Å, and for each step we relax the atoms at the bottom of the tip and at the top of the surface until the forces are smaller than 0.02 eV/Å. The tips used to evaluate the protrusion and hole mode forces on the Pt/TiO_2(110) system are small $(TiO_2)_5$ clusters oriented to expose a singly coordinated O and OH directly pointing to the surface. Such kind of terminations are likely as, during the experiments, tip crashes with the surface are frequent, and an exchange of material between tip and sample is expected. In a previous study [23], we have shown how these two models are capable of reproducing and explaining the force spectroscopy results for the protrusion and hole imaging modes on the h-TiO_2(110) surface. As it also happened in h-TiO_2(110) [23], the relaxations of the tip are crucial to reproduce the forces at short tip-sample distances and to understand why Pt atoms appear as the brighter features in all of the different contrast modes.

III. RESULTS AND DISCUSSION

A. Noncontact AFM images

As discussed in the Introduction, a rich variety of image contrasts has been observed in previous nc-AFM studies of the rutile TiO_2(110) surface [18–23]. Figures 2(a)–2(c) show three typical nc-AFM images recorded in our laboratory for the most frequently observed contrasts of the h-TiO_2(110) surface: protrusion [Fig. 2(a)], hole [Fig. 2(b)], and neutral mode [Fig. 2(c)]. The different appearances of the surface OH defects are marked by black squares on the O_b rows. Alternation between these contrast modes can be obtained with a modification of the tip apex at the single-atom level. The contrast transformation from protrusion to hole imaging modes through some changes in the chemistry of the tip apex is a relatively frequent event, which has been documented previously in the literature [19] and explained recently by means of a hydrogen adsorption that takes place on the lowermost atom of the tip apex [23].

Figures 2(d)–2(f) display, respectively, protrusion mode, hole mode, and neutral mode images of the TiO_2(110) surface, obtained after exposing the hydroxylated surface to the Pt source. The really striking result coming from those images is that Pt atoms appear as bright protrusions in all image contrasts, even when the chemical state of the tip apex changes. We note that the appearance of the Pt atoms in nc-AFM images does not depend on the sample bias voltage applied to minimize the long-range electrostatic forces. This characteristic feature serves as a firm indication of the presence of the Pt and helps to avoid confusion with the H atoms, as the latter appear dissimilar in different imaging contrasts [see Figs. 2(a)–2(c)]. The difference in contrast between Pt and H is surprising as

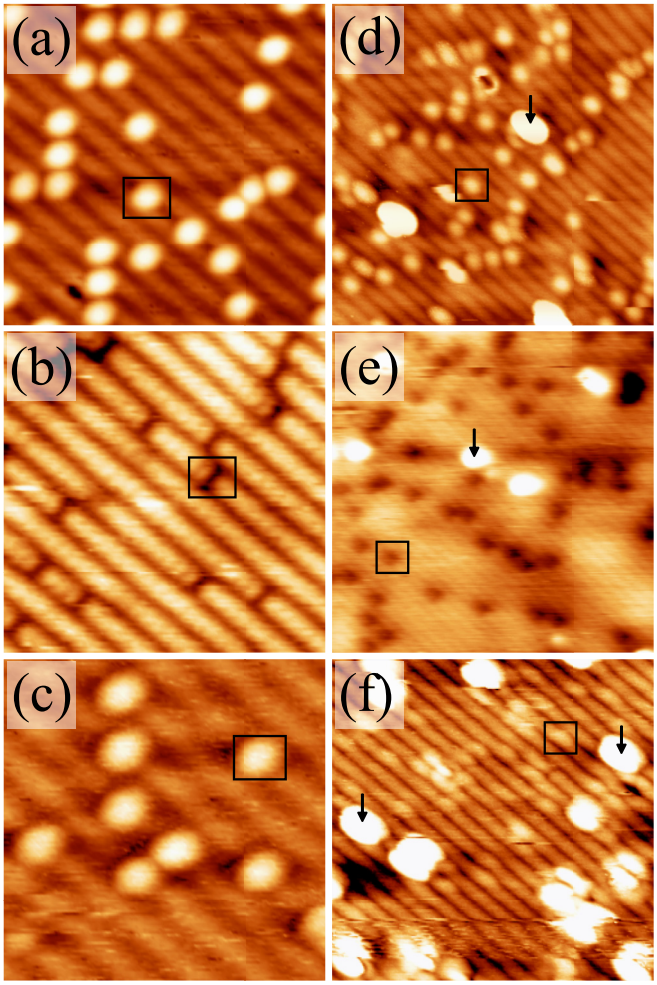

FIG. 2. (Color online) Room-temperature nc-AFM topography images showing the appearance of the Pt atoms deposited on h-TiO_2(110) for the most common image contrasts. (a)–(c) Protrusion mode image (8.25 × 8.25 nm^2), hole mode image (7.25 × 7.25 nm^2), and neutral mode image (4.75 × 4.75 nm^2) for the h-TiO_2(110), respectively. (d)–(f) Protrusion mode image (15 × 15 nm^2), hole mode image (20 × 20 nm^2), and neutral mode image (12.75 × 12.75 nm^2) of the Pt/h-TiO_2(110) surface, respectively. OH defects are highlighted by square boxes. The arrows indicate single Pt atoms. The acquisition parameters were as follows: (a) $f_0 = 163.014$ kHz, $A = 4.8$ nm, $\Delta f = -22.9$ Hz; (b) $f_0 = 166.55$ kHz, $A = 15$ nm, $\Delta f = -0.95$ Hz; (c) $f_0 = 167.44$ kHz, $A = 11.5$ nm, $\Delta f = -0.73$ Hz; (d) $f_0 = 166.42$ kHz, $A = 6.4$ nm, $\Delta f = -14.42$ Hz, $V_s = 0.6$ V; (e) $f_0 = 159.54$ kHz, $A = 14.6$ nm, $\Delta f = -4.6$ Hz, $V_s = 0.95$ V; (f) $f_0 = 167.91$ kHz, $A = 11.5$ nm, $\Delta f = -2.12$ Hz, $V_s = 0.45$ V.

TABLE I. Adsorption energies [in eV, relative to the hollow (H) site] and Pt-O and Pt-Ti bonding distances (in Å) and for Pt adsorbed on different surface sites of TiO_2(110) [see labels in Fig. 3(c)]. Slab model: 2 × 1 surface cell, four O-Ti-O trilayers, two lowermost trilayers fixed to the bulk. The adsorption energy for the H site with this calculation set up is 2.39 eV.

	H	O_{in}	B	Ti_{6f}	O_b	Ti_{5f}
E_{ads} (this work, PBE)	0.0	0.01	0.39	0.26	0.64	1.08
E_{ads} (Ref. [10], PW91)	0.0	0.11	0.13	0.26	0.70	0.95
$d_{Pt\text{-}O}$ (this work)	1.98	1.98		2.04	1.91	
$d_{Pt\text{-}Ti}$ (this work)	2.50	2.72	2.63	2.44		2.37

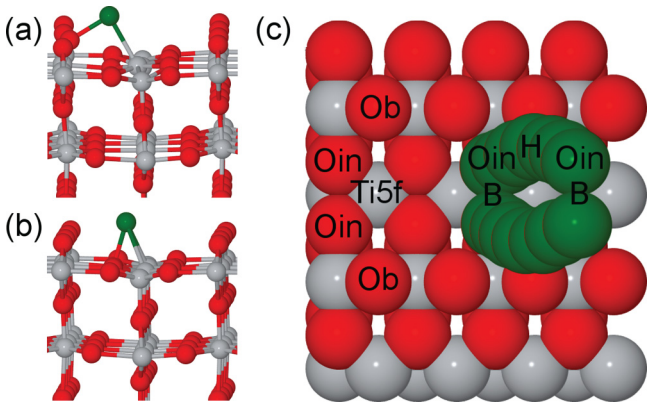

FIG. 3. (Color online) Ball-and-stick structures for Pt atoms adsorbed on TiO_2(110). The same color code of Fig. 1 is used, with Pt atoms represented by green balls. (a) Pt adsorbed on a hollow (H) position, between two O_{in} atoms, with the Pt atom bound to one Ti_{5f} atom and one O_b atom. (b) Pt adsorbed on top of an O_{in} atom, forming bonds with two Ti_{5f} atoms and one O_{in} atom. (c) Top view of the TiO_2(110) surface indicating the different atomic sites and the easy diffusion paths for Pt.

both are electropositive species that tend to act as donors. The evidence for the slightly positively charged Pt on TiO_2 was first presented by Salama *et al.* [29] and further discussed later using kelvin probe force microscopy (KPFM) [30,31]. Both Pt atoms and clusters, deposited on a reduced TiO_2(110), showed small decreases in the local work function, indicative of charge transfer from Pt to the surface. The work function decrease over a single atom is ∼0.25 eV [31], whereas for the clusters [30], the amount of charge per Pt atom was estimated as ⩽ 0.1 electron per Pt atom. Since both H and Pt atoms are positively charged adsorbates on the TiO_2 surface, the diverse appearances of H atoms compared to the invariantly protruding Pt atoms in different image contrasts suggest that a simple model based on electrostatic interactions between a rigid tip apex and surface cannot provide a satisfying explanation to the observed contrast. We will discuss this crucial point further in the following section, when we analyze the results of the force spectroscopy experiments and simulations.

The high resolution topographic appearances of single Pt atoms in various contrast modes provide the possibility to identify the preferential binding sites of Pt atoms on the TiO_2 surface. From the topography contrasts [Figs. 2(d)–2(f)], the Pt atoms appear as elongated features approximately centered on the Ti_{5f} rows and confined between two O_b atomic rows. For the neutral and the protrusion mode [Figs. 2(f) and 2(d), respectively] the location of the Pt features with respect to the atomic rows is most clear. However, in the latter case, the center of the feature is slightly tilted from the center of the Ti_{5f} rows. We can attribute this slight difference to some small change in the tip apex structure, leading to a slightly more asymmetric tip apex for one of the two modes. In addition to single Pt atoms, some larger features visible on the surface may be attributed to either the presence of Pt compounds or Pt dimer structures [see Fig. 2(f)] and will be discussed elsewhere.

The single Pt atoms thus appear to be adsorbed on a region surrounding the Ti_{5f} rows. This is in good agreement with the results of previous theoretical studies of the Pt/TiO_2(110) system [10–12,32,33] and also with the results of our calculations, summarized in Table I, where the relative energies and bonding distances for the different sites are given. All the calculations predict that the hollow site [see the structure in Fig. 3(a) and the site marked as H in Fig. 3(c)] and the O_{in} site [Fig. 3(b), marked as O_{in} in Fig. 3(c)] are the most stable adsorption configurations. Pt is bonded to a Ti_{5f} atom and to an O_b (O_{in}) atom on the H (O_{in}) sites. These two configurations are very close in energy, with the O_{in} site ∼110 meV higher in energy following Iddir *et al.* [10], and almost degenerate with the H site according to our own results. The elongated shape of the Pt atom is also consistent with our calculations and the analysis of the full potential energy surface for Pt on TiO_2(110)-(1 × 1) performed by Iddir *et al.* [10] using a method similar to our theoretical strategy. Pt features seem to span the whole width of the area between two O_b rows and extend for several unit cells. At room temperature, which corresponds to the experimental conditions, and considering the possibility that the tip may further help in reducing the energy barriers between sites, it appears likely that, during the scanning time near the Pt atom, the atom can jump among different sites. The movement along the [001] direction, parallel to the O_b rows, is not significantly limited at RT, as the barrier to overcome is very similar to the difference in binding energies, of the order of 0.1 eV following Iddir *et al.* [10,11] or even smaller according to our results. Thus Pt atom can diffuse easily along one-dimensional channels connecting the hollow and the O_{in} sites [see Fig. 3(c)]. On the other hand, the confinement of the Pt atom movement along the H-O_{in} channels, as encountered in our experiment, might be caused by the surface as well as the subsurface defects [34]. The presence of the surface OH defects limits the migration of Pt atoms on the *h*-TiO_2 surface, allowing one to image isolated single Pt atoms. In the perpendicular direction, the Pt would have to jump over the bridge site [marked as B in Fig. 3(c)] in order to connect the two neighboring channels. This is possible because the limiting barrier that Pt has to overcome in order to move over the bridge site is small, given by the difference between the site energies (∼0.2 eV, following Iddir's work, or ∼0.4 eV, according to our calculations). Energy barriers for jumping over the O_b atoms are significantly larger, confining Pt effectively between the O_b rows.

Our identification of the Pt binding site may appear inconsistent with previous experimental results. Photoemission spectroscopy studies [35] have concluded that, on reduced TiO_2 surfaces and at low coverage, the Pt atoms preferentially

bind on Ti_{5f} sites. This interpretation in the changes of the spectra upon Pt adsorption is not in contradiction with our theoretical results, which indicate that when Pt is adsorbed on any of the most stable adsorption sites, hollow and O_{in} [see Figs. 3(a) and 3(b)], it establishes chemical bonds with the neighboring Ti_{5f} atoms. This reflects in the projected density of states of Pt on TiO_2, as also confirmed by previous theoretical works [12,36]. For the hydroxylated surface, although there is no experimental evidence of such a bond formation upon Pt adsorption, we expect a behavior similar to that described for clean $TiO_2(110)$. In a previous combined nc-AFM and KPFM study of single Pt adsorbates on TiO_2 a single contrast mode, probably protrusion, was observed. All of the bright features were assigned to Pt, concluding that the atom can sit on either the O_b or the Ti_{5f} rows [31]. We think that the features on the O_b rows might have been some H adsorbates which were confused with Pt atoms. In our case, the access to the different imaging modes is crucial in order to provide an unambiguous identification of the Pt adsorbates.

B. Force spectroscopy curves

To get further insight into the nature of the tip-sample interaction and the contrast mechanisms, we measured the force versus distance curves over different surface sites for the two most frequent contrast modes. Figure 4(a) displays one of our set of forces corresponding to a protrusion mode tip over the two brightest surface sites, Pt and OH. The forces over the Pt atom are characterized by a minimum of ~ -1.1 nN and those over the OH group are systematically smaller, with a minimum at about -0.45 nN. The magnitude of the force minimum over the OH site is slightly smaller than the one obtained in our previous measurements at 80 K [23]. This small change might be associated with a thermally activated relaxation affecting the atomic positions at room temperature. Such kind of events have been described previously in the literature [37]. Although absolute values of force magnitude have some variability, in all our experiments the forces over Pt were systematically larger than those over OH for the full distance range, implying that Pt atoms always have a brighter nc-AFM contrast than the other atoms (O,Ti) in the surface. The relative position of the force minima associated with the OH and the Pt sites is also very reproducible for different experiments. The distance difference is about ~ 1.5 Å, with the OH minimum appearing at shorter distances.

The results of our simulations with the O-terminated tip, see Fig. 4(b), are consistent with the trends observed in the experiments. The shape of the tip-sample interaction curves nicely follows the one extracted from the experiments, with forces on the Pt site larger than those on the OH site for the whole distance range, and a crossing at a distance close to the OH force minimum. The magnitude of the force is well reproduced for the OH site, with a maximum attractive force of ~ 0.55 nN that is slightly larger than the one found in the experiment, but is clearly overestimated for the Pt atom. We have explored different alternatives but failed to provide a completely satisfactory explanation for this discrepancy between theory and experiment. First, we have tried other tip models. The best candidate, with somewhat smaller forces on the Pt site, is the doubly coordinated O-terminated tip model used in our previous study of the $TiO_2(110)$ surface [23]. This tip reproduces the important trends, including the relative position of the force minima discussed below, but still gives us forces over the Pt site that, although smaller than those in Fig. 4(b), are too large compared to the experiment. We believe that a very blunt tip is responsible for the observed discrepancy in the maximum attractive forces. While such a tip can provide an image contrast similar to that obtained with a sharp tip, the influence of blunt tip appears at closer tip-sample distances around maximum attractive force. At such close distances, while the foremost atom of the apex interacts with Pt atom, the neighboring O atoms over the tip apex may interact with the surface O_b atoms. Thus an additional repulsive interaction with neighboring O_b atoms can occur. The resulting repulsive force reduces the attractive interaction force between tip and Pt atoms.

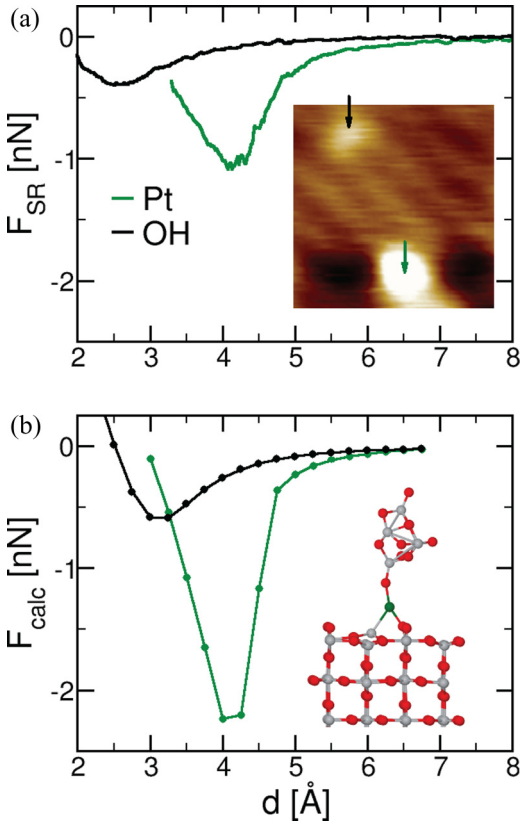

FIG. 4. (Color online) Tip-sample forces for the protrusion mode imaging contrast of $Pt/TiO_2(110)$. (a) Experimental short-range forces over Pt (green line) and OH (black line). Inset: nc-AFM image of the surface region where the forces were measured. The green and black arrows indicate the Pt and OH sites where measurements were taken. The acquisition parameters were as follows: $f_0 = 160.17$ kHz, $A = 12.3$ nm, $\Delta f = -1.61$ Hz. KPFM parameters: $U_{ac} = 0.5$ V, $f_{ac} = 500$ Hz. Image size: 3.5×3.5 nm^2. The tip-sample distance in the experimental curves has been shifted to align the attractive force minima of Pt atom with the theoretical calculations. (b) Calculated forces over Pt and OH, with the same color code. Inset: tip-sample structure over the Pt site at $d = 4.25$ Å. In our calculations, the Pt is adsorbed on the most stable site [hollow; see Figs. 3(a) and 3(c)].

The larger forces on the Pt site and the relative position of the force minima, appearing in Pt at distances which are

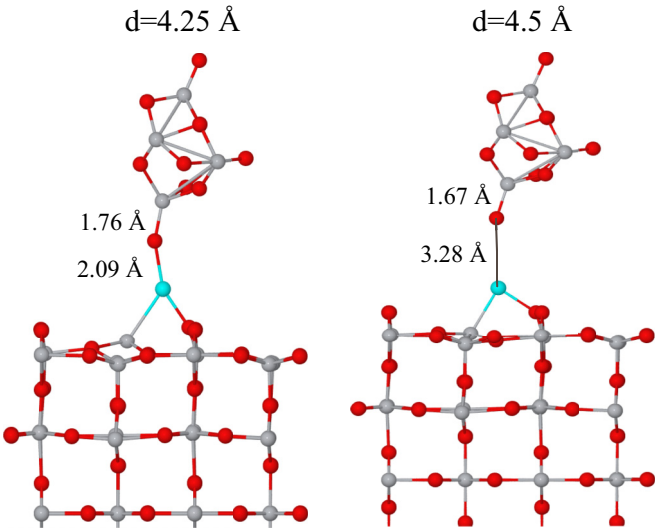

FIG. 5. (Color online) Tip-sample relaxations induced by the interaction with an O-terminated tip. The structures over the Pt site at $d = 4.25$ and 4.5 Å illustrate the large upward displacement of the Pt ($\sim$1 Å over the O_b surface atoms) associated with the strong chemical interaction with the O atom at the tip apex. This relaxation explains the relative position of the force minima on the Pt and OH sites.

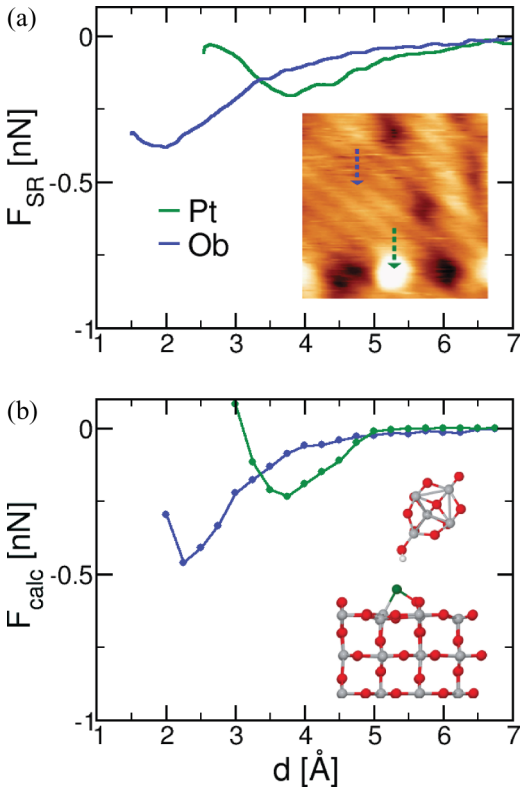

FIG. 6. (Color online) Tip-sample forces for the hole imaging mode of Pt/TiO_2(110) surface. (a) Experimental short-range forces over Pt (green line) and O_b (blue line). Inset: nc-AFM image of the surface region where the forces were measured, with the green and blue arrows indicating the Pt and O_b sites where the forces were measured. The tip-sample distance in the experimental curves has been shifted to align the attractive force minima of Pt atom with the theoretical calculations. The acquisition parameters were as follows: $f_0 = 158.33$ kHz, $A = 16.9$ nm, $\Delta f = -2.12$ Hz, $V_s = 1.0$ V. Image size: 5.5×5.5 nm^2. (b) Calculated forces over Pt and O_b, with the same color code. Inset: tip-sample structure over the Pt site at $d = 3.0$ Å. The Pt atom is adsorbed on a hollow site (as in Fig. 4).

significantly larger [$\sim$1 (1.5) Å according to simulations (experiment)] than that over OH, is particularly striking considering that both adsorbates, H and Pt, protrude similarly with respect to the O_b atoms ($\sim$1 Å). The key elements to understand these two effects are the intrinsic strength of the Pt-O interaction—a clear indication of the chemical reactivity of the Pt adsorbates—and the strong atomic relaxations that take place when the Pt from the surface and the O from the tip start to interact chemically. These relaxations are illustrated in Fig. 5, where the structures for $d = 4.50$ and $d = 4.25$ Å (close to the force minimum) are displayed. The interaction is strong enough to raise the Pt atom about 1 Å over the O_b surface atoms, pulling the Ti_{5f} atom bonded to it. The resulting Pt-O distance ($\sim$2 Å) is in the range characteristic of Pt-O bonds (see Table I), indicating the formation of a chemical bond. No significant relaxation takes place on the OH site, and thus the force minima appear shifted 1 Å from each other. Notice that the experimental distance between the minima is somewhat larger, $\sim$1.5 Å. We attribute the underestimation of this distance in the calculation to the limited description of the tip elastic response provided by our tip model, where only the four atoms closer to the apex are allowed to relax under the tip-sample interaction.

We also measured the forces for hole mode imaging tips. In Fig. 6(a), we show one representative set of observed forces over Pt and O_b, which are the two brightest atoms in this imaging mode. In this case, the interactions between the tip and the imaged atoms are weaker, with force minima of ~ -0.25 nN and -0.38 nN for Pt and O_b, respectively. The minimum over Pt appears at larger distances (about $\sim$1.75 Å larger) than that for O_b. The reproducibility of these trends in different measurements is also very good, with just slight changes in the distance difference between two force minima. The forces are systematically larger over the Pt site for medium to large distances, and this can be connected to the puzzling fact that the Pt is the brightest atom of the surface also in the hole mode.

In order to explain the contrast associated with the Pt adsorbates, we have performed force calculations with our OH-terminated, TiO_2-based nanoapex approaching the two brightest sites: Pt and O_b. We have obtained forces in very good agreement with the results of the experiments [see Fig. 6(b)]. The two calculated minima are of similar magnitude to the observed ones, and their relative location is also well reproduced. As discussed in our previous study on the h-TiO_2(110) surface [23], the interaction over the O_b site is essentially due to hydrogen bonding. The interaction over the Pt site appears to be of electrostatic nature. The OH bond of the tip bends with the O staying on top of the Pt and the H lying out of that line [see inset of Fig. 6(b)] to maximize the electrostatic interactions between the nearest H, O, and Pt ions. This is the same mechanism responsible for the interaction with the Ti_{5f} sites discussed in Ref. [23]. In that case the maximum attractive

force was comparable to the one on the O_b, while in the case of Pt, it is approximately half of that value. We can trace back the reduced strength of the interaction to differences in the effective charges of the two metallic species. Bader charge analysis for the case where the Pt atom is adsorbed on a hollow site gives values of +0.12, +2.16, and −1.08 electrons for Pt, Ti (average), and O (average), respectively. These charges are not modified significantly by the presence of the tip.

The main reason for the brighter appearance of the Pt atom appears to be the surface topography: the Pt atom is about 1 Å higher than the O_b. This height difference, combined with the relaxations induced by the tip-sample interaction, are responsible for the appearance of the force minimum over Pt at 1.5 Å further away from the surface than on the O_b site, in good agreement with the experiment. For relatively short tip-sample distances, the calculations predict that force curves for Pt and O_b cross, leading to a contrast inversion with O_b atoms appearing brighter. Experimental force curves also support this contrast inversion, but, as in the protrusion case, we were not able to collect images in that distance range.

IV. CONCLUSIONS

We have presented a study of single Pt atoms adsorbed on h-$TiO_2(110)$ based on nc-AFM and complemented with DFT simulations which help to interpret the results. We have obtained high-resolution images of the surface for the most frequent contrast modes, and all of them indicate that the Pt atom can be distinguished from the H adsorbate due to its characteristic shape and binding site (near the Ti_{5f} rows), and, particularly, because it is the brightest atom of the surface for all contrast modes. The nc-AFM results are consistent with the DFT picture of the adsorption and diffusion of Pt on $TiO_2(110)$ and also with previous experimental works. The region for adsorption and diffusion of Pt is that surrounding the fivefold coordinated Ti atoms and confined between two O_b atomic rows. It appears that the microscope tip helps to lower some diffusion barriers. We have also presented force spectroscopy data for the protrusion and hole imaging modes and calculated tip-sample forces that are in very good agreement with the observations. This provides further support to the tip models used in this study, which were recently proposed to explain the force spectroscopy of h-$TiO_2(110)$, and are expected to be useful to study other adsorbates and defects on TiO_2 and other oxide surfaces. Recent work of some of us on the identification of chemical species and the characterization of defects on the anatase $TiO_2(101)$ surface by simultaneous scanning tunneling and atomic force microscopy confirms that OH-terminated TiO_2 nanoclusters are useful tip models to understand AFM imaging on these materials [38].

From the comparison between the experimental and the calculated forces we have unveiled the imaging mechanisms for Pt on the surface, and explained why it is the brightest surface atom in the two contrast modes. This puzzling result comes from a combination of the intrinsic strength of the interaction with the Pt adatom—that reflects its chemical reactivity and explains the important role it plays in catalysis—and the relaxations induced by the tip-sample interaction. In the protrusion mode, a chemical bond between Pt and the O atom in the tip apex starts to form, and the effect is enhanced by a tip-induced displacement that pushes the Pt atom almost 1 Å out from the surface, and singles it out from the OH defect. In the hole imaging mode, a lateral deflection of the H terminal atom exposes the O and makes the forces attractive over the Pt site. This interaction is weaker than in the protrusion mode due to the screening of the H atom but still strong enough to induce an upward displacement of the Pt atom by 0.5 Å. This relaxation sums up to the 1 Å height difference of Pt and O_b sites, to explain the relative position of the force minima in the spectroscopy curves and the fact that Pt represents the brighter feature for the range of distances where nc-AFM imaging is usually performed. We expect other positively charged metallic adsorbates on TiO_2 to have nc-AFM contrasts and tip-sample interaction mechanisms similar to those described here for the Pt adsorbate. One of such cases is the K adsorbate, which has been reported to appear as a bright protrusion for various nc-AFM contrast modes [34]. Thus the AFM contrast for Pt and other metallic species seems to reflect its chemical reactivity and provides an explanation for the important role they play in catalysis. This supports the use of AFM not only to characterize their adsorption structure but also to directly probe their chemical activity.

ACKNOWLEDGMENTS

This work was supported by Grants-in-Aid for Scientific Research (No. 22221006, No. 25106002, No. 24360016, No. 26600099, No. 26600015, No. 26110516, and No. 20760024) from the Ministry of Education, Culture, Sports, Science and Technology (MEXT) of Japan, Funding Program for Next Generation World-Leading Researchers and by the Ministerio de Economia y Competitividad (MINECO, Spain) under Projects No. MAT2011-23627, No. CSD2010-00024, and No. PLE2009-0061. Computer time provided by the Spanish Supercomputing Network (RES) in the Barcelona Supercomputer Center (MareNostrum III) and the CesViMa (Magerit) is gratefully acknowledged.

[1] F. E. Osterloh, Chem. Mater. **20**, 35 (2008).
[2] O. K. Varghese, M. Paulose, T. J. LaTempa, and C. A. Grimes, Nano Lett. **9**, 731 (2009).
[3] S. Gan, Y. Liang, D. R. Baer, M. R. Sievers, G. S. Herman, and C. H. F. Peden, J. Phys. Chem. B **105**, 2412 (2001).
[4] S. J. Yoo, T.-Y. Jeon, K.-S. Lee, K.-W. Park, and Y.-E. Sung, Chem. Commun. **46**, 794 (2010).
[5] K. Yamamoto, T. Imaoka, W.-J. Chun, O. Enoki, H. Katoh, M. Takenaga, and A. Sonoi, Nat. Chem. **1**, 397 (2009).
[6] S. Bonanni, K. Aït-Mansour, H. Brune, and W. Harbich, ACS Catal. **1**, 385 (2011).
[7] S. Bonanni, K. Aït-Mansour, W. Harbich, and H. Brune, J. Am. Chem. Soc. **136**, 8702 (2014).

[8] T.-Y. Chang, Y. Tanaka, R. Ishikawa, K. Toyoura, K. Matsunaga, Y. Ikuhara, and N. Shibata, Nano Lett. **14**, 134 (2014).
[9] U. Diebold, Surf. Sci. Rep. **48**, 53 (2003).
[10] H. Iddir, S. Öğüt, N. D. Browning, and M. M. Disko, Phys. Rev. B **72**, 081407(R) (2005).
[11] H. Iddir, S. Öğüt, N. D. Browning, and M. M. Disko, Phys. Rev. B **73**, 039902(E) (2006).
[12] V. Çelik, H. Ünal, E. Mete, and S. Ellialtıoğlu, Phys. Rev. B **82**, 205113 (2010).
[13] S. Morita, F. Giessibl, and R. Wiesendanger, *NCAFM Vol. 2* (Springer, New York, 2009).
[14] R. García and R. Pérez, Surf. Sci. Rep. **47**, 197 (2002).
[15] J. V. Lauritsen and M. Reichling, J. Phys.: Condens. Matter **22**, 263001 (2010).
[16] C. Barth, A. S. Foster, C. R. Henry, and A. L. Shluger, Adv. Mater. **23**, 477 (2011).
[17] M. Z. Baykara, M. Todorović, H. Mönig, T. C. Schwendemann, O. Ünverdi, L. Rodrigo, E. I. Altman, R. Pérez, and U. D. Schwarz, Phys. Rev. B **87**, 155414 (2013).
[18] J. V. Lauritsen, A. S. Foster, G. H. Olesen, M. C. Christensen, A. Kühnle, S. Helveg, J. Rostrup-Nielsen, B. S. Clausen, M. Reichling, and F. Besenbacher, Nanotechnology **17**, 3436 (2006).
[19] G. H. Enevoldsen, A. S. Foster, M. C. Christensen, J. V. Lauritsen, and F. Besenbacher, Phys. Rev. B **76**, 205415 (2007).
[20] G. H. Enevoldsen, H. P. Pinto, A. S. Foster, M. C. R. Jensen, A. Kühnle, M. Reichling, W. A. Hofer, J. V. Lauritsen, and F. Besenbacher, Phys. Rev. B **78**, 045416 (2008).
[21] R. Bechstein, C. González, J. Schtte, P. Jelínek, R. Pérez, and A. Kühnle, Nanotechnology **20**, 505703 (2009).
[22] A. Yurtsever, Y. Sugimoto, M. Abe, and S. Morita, Nanotechnology **21**, 165702 (2010).
[23] A. Yurtsever, D. Fernández-Torre, C. González, P. Jelínek, P. Pou, Y. Sugimoto, M. Abe, R. Pérez, and S. Morita, Phys. Rev. B **85**, 125416 (2012).
[24] T. Albretch, P. Grütter, D. Horne, and D. Rugar, J. Appl. Phys. **69**, 668 (1991).
[25] F. Rieboldt, L. B. Vilhelmsen, S. Koust, J. V. Lauritsen, S. Helveg, L. Lammich, F. Besenbacher, B. Hammer, and S. Wendt, J. Chem. Phys. **141**, 214702 (2014).
[26] J. E. Sader and S. P. Jarvis, Appl. Phys. Lett. **84**, 1801 (2004).
[27] J. P. Perdew, K. Burke, and M. Ernzerhof, Phys. Rev. Lett. **77**, 3865 (1996).
[28] G. Kresse and J. Furthmüller, Phys. Rev. B **54**, 11169 (1996).
[29] T. M. Salama, H. Hattori, H. Kita, K. Ebitani, and T. Tanaka, J. Chem. Soc., Faraday Trans. **89**, 2067 (1993).
[30] A. Sasahara, C. L. Pang, and H. Onishi, J. Phys. Chem. B **110**, 17584 (2006).
[31] A. Sasahara, C. L. Pang, and H. Onishi, J. Phys. Chem. B **110**, 13453 (2006).
[32] S. Yongprapat, S. Therdthianwong, and C. Kritayakornupong, Comput. Mater. Sci. **44**, 536 (2008).
[33] E. Mete, O. Gülseren, and Ş. Ellialtıoğlu, Eur. Phys. J. B **85**, 204 (2012).
[34] A. Yurtsever, Y. Sugimoto, M. Abe, K. Matsunaga, I. Tanaka, and S. Morita, Phys. Rev. B **84**, 085413 (2011).
[35] K. Schierbaum, S. Fischer, M. Torquemada, J. de Segovia, E. Román, and J. Martin-Gago, Surf. Sci. **345**, 261 (1996).
[36] D. Cheng, J. Lan, D. Cao, and W. Wang, Appl. Catal. B: Environ. **106**, 510 (2011).
[37] H. Nejat Pishkenari and A. Meghari, Int. J. Mod. Phys.: Conf. Ser. **05**, 418 (2012).
[38] R. Pérez and O. Custance (private communication).